Transition of velocity distributions in collapsing self-gravitating N-body systems

Transition of velocity distributions in collapsing self-gravitating N-body systems

Nobuyoshi Komatsu,[1,*] Takahiro Kiwata,[1] and Shigeo Kimura[2]

[1]*Department of Mechanical Systems Engineering, Kanazawa University, Kakuma-machi, Kanazawa, Ishikawa 920-1192, Japan*

[2]*The Institute of Nature and Environmental Technology, Kanazawa University, Kakuma-machi, Kanazawa, Ishikawa 920-1192, Japan*

(Received 21 June 2011; revised manuscript received 19 August 2011; published 22 February 2012)

By means of N-body simulations, we study the evolution of gravity-dominated systems from an early relaxation to a collapse, focusing on the velocity distributions and thermodynamic properties. To simulate the dynamical evolution, we consider self-gravitating small N-body systems enclosed in a spherical container with adiabatic or semipermeable walls. It is demonstrated that in the early relaxation process, the velocity distribution is non-Gaussian and q-Gaussian, since the system is in quasiequilibrium states (here q is the Tsallis entropic parameter). Thereafter, the velocity distribution undergoes higher non-Gaussian distributions, especially when the core forms rapidly in the collapse process; i.e., q tends to be larger than that for the quasiequilibrium state, since the velocity distribution further deviates from Gaussian. However, after the core forms sufficiently, the velocity distribution gradually relaxes toward a Gaussian-like distribution. Accordingly, the velocity distribution evolves from a non-Gaussian distribution through a higher non-Gaussian distribution to a Gaussian-like distribution; i.e., the velocity distribution does not monotonically relax toward a Gaussian-like distribution in our collapse simulations. We clearly show such a transition of the velocity distribution, based not only on the Tsallis entropic parameter but also on the ratio of velocity moments. We also find that a negative specific heat occurs in a collapse process with mass and energy loss (such as the escape of stars from globular clusters), even if the velocity distribution is Gaussian-like.

DOI: 10.1103/PhysRevE.85.021132 PACS number(s): 05.20.−y, 05.70.−a, 45.50.Jf, 95.30.Tg

I. INTRODUCTION

Self-gravitating or long-range attractive interacting systems exhibit several peculiar features [1–4], such as gravothermal catastrophe [5,6], negative specific heat [7–9], violent relaxation [10], nonequilibrium thermodynamics, and nonextensive statistical mechanics [11–30]. In these systems, the velocity distributions are non-Gaussian [31–33], especially in quasiequilibrium states and metastable states. For example, Iguchi *et al*. proposed universal non-Gaussian velocity distributions for a spherical collapse in a violent gravitational process of a collisionless stage ($t < \tau_r$) [32], and Carvalho *et al*. indicated that the q parameter in the Tsallis distribution depends on the age of open stellar clusters [33]. (Here τ_r represents the relaxation time, which is driven by the two-body encounter [1]). On the other hand, Gaussian and Maxwell-Boltzmann velocity distributions have been discussed in core-halo states in a collisional stage ($t \gg \tau_r$) by Ispolatov *et al*. [34], and the velocity distribution was examined in the central region of bound particles in a collapse process by Merrall *et al*. [35]. These works suggest that after undergoing a quasiequilibrium state in the collisionless stage, gravity-dominated systems should finally relax toward a Boltzmann-like state in the collisional stage through a collapse process, even if the system does not approach the exact thermodynamic equilibrium state. That is, time scales and energy states affect the dynamical evolution of self-gravitating N-body systems and, therefore, a finite lifetime of metastable states [36–39] and phase transitions [40–50] have been examined from the viewpoint of thermodynamics.

However, velocity distributions have not yet been extensively discussed in long-term nonequilibrium processes, except for a few studies [1,32–35], although they should play an important role in the thermodynamic properties of a system. In other words, it is not yet understood completely how the velocity distribution evolves from an early relaxation to a collapse. (Density profiles and energy distributions have been extensively examined from an astrophysical viewpoint; e.g., see Refs. [1,2] and references therein.) We expect that an understanding of the evolution of the velocity distribution can give new insight into the thermodynamics of the nonequilibrium process in long-range attractive interacting systems. Accordingly, we have investigated the evolution of a self-gravitating N-body system, focusing on the velocity distributions and thermodynamic properties [51]. (Recently, Latora *et al*. [52], Pluchino *et al*. [53] and Chavanis *et al*. [54–56] have investigated the phase transition and relaxation of self-gravitating systems, using Hamiltonian mean-field models for one-dimensional systems.)

In the present study, we examine two collapse models for a self-gravitating N-body system enclosed in a spherical container with reflecting walls. As shown in Fig. 1(a), we first consider a "cold collapse process" under a restriction of constant mass and energy using adiabatic walls, because a system enclosed in a spherical container is suitable for examining the fundamental characteristics of the thermodynamic properties [15,29,34]. (To simulate the cold collapse process, we employ a typical small N-body system which has been analyzed in detail [34,48], since the well-studied system is an important benchmark system for examining a collapse theoretically and numerically.) Of course, even high-energy particles cannot escape from the spherical container in the above model. In fact, the escape of stars from globular clusters or the so-called evaporation process can drive the cluster toward a configuration with a high-density core [57]. Therefore, to mimic such mass and energy loss, we also consider an evaporation process using semipermeable reflecting walls, as

*komatsu@t.kanazawa-u.ac.jp

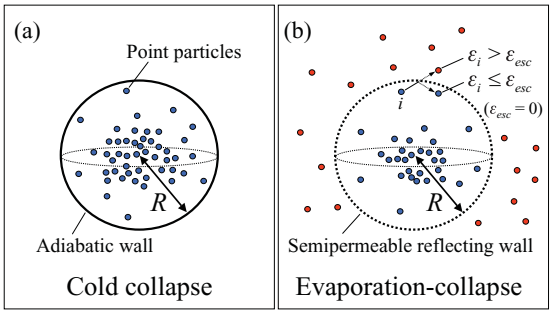

FIG. 1. (Color online) Two models for collapse processes. (a) Cold collapse process under a restriction of constant mass and energy. (b) Evaporation-collapse process with mass and energy loss. For the cold collapse process, an adiabatic wall is employed and the initial temperature is set to be sufficiently low. For the evaporation-collapse process, the particle passes through a semipermeable reflecting wall freely when the total energy ε_i of the ith particle exceeds an energy threshold $\varepsilon_{\rm esc}$ [30]. In this study, $\varepsilon_{\rm esc}$ is set to be 0. For details, see the text in Sec. II B.

previously suggested by the present authors [30] and shown in Fig. 1(b). (Hereafter, we call this an "evaporation-collapse process," since the system should undergo a collapse.)

The present paper is organized as follows. In Sec. II, we give a brief review of numerical methods for simulating self-gravitating N-body systems. In Sec. II A, we describe simulation techniques for a system enclosed in a spherical container with reflecting walls. In Sec. II B, we introduce two models for collapse simulations using adiabatic and semipermeable walls. In Sec. II C, we describe several parameters, e.g., the virial ratio, the ratio of velocity moments, and the Tsallis entropic parameter. In Sec. III, we present the simulation results of two collapse processes. In Sec. III A, we examine a cold collapse process with constant mass and energy. In Sec. III B, we investigate an evaporation-collapse process with mass and energy loss. We also discuss the correlation between the Tsallis entropic parameter and the ratio of velocity moments. Moreover, we observe the energy distributions and the density-velocity correlations in typical collapse processes. Finally, in Sec. IV, we present our conclusions.

II. METHODS

A. Simulation techniques

In this study, we consider a system consisting of N point particles enclosed in a spherical container of radius R with reflecting walls. As shown in Fig. 1, we examine two collapse models: (1) a cold collapse process under a restriction of constant mass and energy and (2) an evaporation-collapse process with mass and energy loss. In the present paper, to mimic a cold collapse, the initial kinetic energy is set to be negligible values smaller than the order of 1% of the total energy. We call this the "cold collapse." The details for the models are given in Sec. II B.

To simulate the two processes, we integrate a set of classical equations of motion for the particles interacting through the Plummer softened potential [1–3]:

$$\Phi = -1/\sqrt{r^2 + r_0^2}, \tag{1}$$

where r and r_0 represent the distance between particles and the softening parameter, respectively. The total energy E^w of the whole system is defined as

$$E^w = E^w_{\rm KE} + E^w_{\rm PE} = \sum_i^N \frac{m_i v_i^2}{2} - \sum_{i<j}^N \frac{G m_i m_j}{\sqrt{r_{ij}^2 + r_0^2}}, \tag{2}$$

where $E^w_{\rm KE}$, $E^w_{\rm PE}$, and m_i represent kinetic energy, potential energy, and mass of the ith point particle, respectively [30]. G, v_i, and r_{ij} represent the gravitational constant, the speed of the ith particle, and the distance between the ith and jth particles, respectively. The mass m_i of each particle is set to be m. The superscript notation w represents a value of the whole system, since a high-energy particle passes through the semipermeable reflecting wall in our evaporation-collapse process [30]. That is, in the evaporation-collapse process, the number N_s ($r_i, r_j < R$) of particles in the sphere decreases from the number N of particles in the whole system. Of course, N_s is equal to N during the cold collapse process, because of the adiabatic walls. In this paper, we investigate the properties of the system in the sphere and, therefore, we consider the system within the semipermeable reflecting wall as an open system. We define the total energy E in the sphere, substituting N_s into N in Eq. (2) [30]. (In the cold collapse process, E is equal to E^w, since N_s is equal to N.)

The total rescaled energy ε in the sphere is defined as

$$\varepsilon = \varepsilon_{\rm KE} + \varepsilon_{\rm PE} = E\frac{R}{GM_s^2} = E\frac{R}{G(mN_s)^2}, \tag{3}$$

where M_s represents the total mass in the sphere and $\varepsilon_{\rm KE}$ and $\varepsilon_{\rm PE}$ represent the rescaled kinetic and potential energies in the sphere, respectively [30]. In this study, the units of time t and velocity v are $\sqrt{R^3/(Gm)}$ and $\sqrt{Gm/R}$, respectively [29]. The units are set to be $G = R = m = 1$, to ensure generality of the system. Therefore, ε depends on the temporal energy E and the temporal number N_s of particles in the sphere. In our units, the temperature T of the system in the sphere is given by

$$T = \frac{2}{3k_B}\varepsilon_{\rm KE} = \frac{2}{3}\varepsilon_{\rm KE}, \tag{4}$$

assuming that the kinetic energy corresponds to the temperature and that Boltzmann's constant $k_B = 1$.

In our simulations, r_0 for the Plummer softened potential is set to be $0.005R$ [29,30], which is sufficiently smaller than the critical value $0.021R$, above which the collapse-explosion transition is replaced by a normal first-order phase transition [34,47]. The collapse energy for the system with an adiabatic wall is $\varepsilon_{\rm coll} \approx -0.339$ [34], which means that if ε of a uniform state becomes lower than $\varepsilon_{\rm coll}$, the system should undergo a collapse to a core-halo state.

In the present study, we consider a system consisting of $N = 125$–250 point particles inside and outside a spherical container of $R = 1$. For simulating an N-body system, the set of equations of motion is integrated using Verlet's algorithm, as for our previous studies [29,30]. To maintain the accuracy of our simulations, a time step of $\Delta t = 10^{-5}$ or $\Delta t = 0.5 \times 10^{-5}$ is selected, based on a simulation with several different time steps [29,30,58]. (Since Verlet's algorithm is a third-order symplectic integrator, higher-order symplectic integrators are

required to select a larger time step.) The results are averaged over 30 simulations, to determine the averaged behavior of the system. Therefore, incoherent phenomena, e.g., gravothermal oscillations, are not observed clearly in this study.

In self-gravitating N-body systems, two time scales are typically discussed, the crossing time τ_c, corresponding to the free-fall time, and the relaxation time τ_r, which is driven by the two-body encounter. The two time scales are evaluated as $\tau_c \approx 1/\sqrt{G\rho}$ and $\tau_r \approx (0.1N/\ln N)\tau_c$, respectively, where ρ represents the density assuming a uniform density profile [1,25]. In our units, τ_c and τ_r for the present system of $N = 125$ (or $N = 250$) are evaluated as $\tau_c \approx 0.2$ (or $\tau_c \approx 0.1$) and $\tau_r \approx 0.5$ (or $\tau_r \approx 0.6$), respectively. However, it takes a much longer time for the collapse to be complete in a core-halo state. For example, the complete collapse time in a system with $N = 100$–200 particles is approximately 10^3–10^4 τ_c [48] and, therefore, the collapse time of the present study is evaluated as being of the order of 10^2–10^3 in our units. (The collapse time for the evaporation-collapse process should be slightly shorter than the above value, since N_s decreases to $\sim$20 in our evaporation-collapse simulation.) Note that we do not discuss the system in the complete core-halo state.

To simulate the cold collapse process, we employ a typical small N-body system which has been analyzed in detail [34,48], i.e., the system consisting of 125 particles enclosed in a spherical container with adiabatic walls. This is because the well-studied system is an important benchmark system for examining a collapse theoretically and numerically. Therefore, in this paper, we first examine the cold collapse process step-by-step, by comparing with the result in Ref. [34]. To this end, several parameters for our simulations, e.g., the number N of particles, the softening parameter r_0, and the criteria of the core r_c (discussed in Sec. II C), are set to be the same as Ref. [34]. The details of our models are summarized in the next subsection.

B. Numerical models

1. Cold collapse process with constant mass and energy

Spherical adiabatic walls are employed to simulate a cold collapse process under a restriction of constant mass and energy, as shown in Fig. 1(a). In this model, the radial component of the velocity of a particle is reversed when it reaches the adiabatic wall [58]. To mimic a cold collapse, the initial temperature is set to be sufficiently low in nonequilibrium states. For the initial setup, we prepare the initial density profiles and velocities as follows.

For the initial density profile, we assume a radial density profile based on the Plummer model, $\rho(r) \propto (1 + r^2/a^2)^{-5/2}$ [1,2]. The Plummer density profile is determined from the initial potential energy. The initial potential energy $\varepsilon_{\rm PE0}$ is set to be negligible, lower than the target total energy, since the initial kinetic energy $\varepsilon_{\rm KE0}$ is sufficiently small for the cold collapse (Table I). To distribute the particles in the spherical container of radius $R = 1$, the container is first divided into 10 spherical shells in the radial direction r, where the distance between the inner and outer shells is set to be $\Delta r = 0.1$ [58]. Based on the density profile of the Plummer model, the particles are distributed randomly in the spherical shells, taking into account the spherically symmetric profile.

TABLE I. Initial setup of the cold collapse process with constant mass and energy. The errors indicate the 68% confidence level in terms of the normal error distribution using 30 simulations.

ε	$\varepsilon_{\rm PE0}$	$\varepsilon_{\rm KE0}$
-0.6	-0.602 ± 0.001	0.002 ± 0.001
-0.8	-0.802 ± 0.001	0.002 ± 0.001
-1.0	-1.002 ± 0.002	0.002 ± 0.002
-1.2	-1.203 ± 0.002	0.003 ± 0.002

We set the initial velocity $|\mathbf{v}_0|$ to be sufficiently small so that $2\varepsilon_{\rm KE0}/|\varepsilon_{\rm PE0}| < 0.01$. That is, we assume that the initial velocity is that of a nonequilibrium state. For our initial setup, all the particles are set to have a small velocity with equal $|\mathbf{v}_0|$ but with a random direction, keeping the target total energy ε and $2\varepsilon_{\rm KE0}/|\varepsilon_{\rm PE0}| < 0.01$. Thereafter, to keep the total momentum and total angular momentum equal to 0, the velocities of the particles are slightly modified, taking into account the subsequent density profile. These operations are iterated until the total energy of the system approaches the target total energy. Therefore, the obtained density profiles are slightly different from those for the Plummer model. We have confirmed that our main results in the present study are not influenced much by such a small difference in the initial density profiles or in the initial velocity distributions.

In our cold collapse simulation, $N = 125$. To examine the influence of the total energy, ε is set to -0.6, -0.8, -1.0, and -1.2, respectively. The total energy is sufficiently smaller than the collapse energy, $\varepsilon_{\rm coll} \approx -0.339$. The simulation time is set to 300–400 in our units. The details for the initial setup are summarized in Table I.

Self-gravitating systems for $-1 \lessapprox \varepsilon \lessapprox 1$ have been extensively examined from a thermodynamic viewpoint, since the thermodynamic properties rapidly vary [25,26,29,30,34]. In this study, we examine the cold collapse process of the system for $\varepsilon = -0.6 \sim -1.2$, to observe variations in velocity distributions clearly. This is because we expect that the variation in velocity distributions increases with increasing negative energy. Moreover, for $\varepsilon = -0.6 \sim -1.2$, the velocity distribution approaches a Gaussian-like distribution in a reasonable time scale (and a reasonable computational time). Therefore, in the present paper, we do not discuss the lifetime of metastable states close to $\varepsilon_{\rm coll}$. (Note that the lifetime of the metastable state is an important and unresolved issue of the collapse processes. For example, it has been theoretically discussed that a typical lifetime of the metastable state should depend on the number N of particles and on the offset of the energy from the collapse energy, $\varepsilon - \varepsilon_{\rm coll}$ [38]. However, the details remain unresolved.)

2. Evaporation-collapse process with mass and energy loss

For an evaporation-collapse process with mass and energy loss, we employ semipermeable reflecting walls, as shown in Fig. 1(b). We give a brief review of this model, according to Ref. [30]. In this model, when the total energy ε_i of the ith particle in the sphere exceeds an energy threshold $\varepsilon_{\rm esc}$, the particle freely passes through the semipermeable reflecting wall as if there was no wall. In contrast, when ε_i is equal to or

smaller than $\varepsilon_{\rm esc}$, i.e., $\varepsilon_i \leqq \varepsilon_{\rm esc}$, the spherical wall behaves like an adiabatic wall. Usually, the energy threshold $\varepsilon_{\rm esc}$ should be 0, since the particle can escape from the system when its kinetic energy is larger than the potential energy. To calculate the rescaled energy ε_i, the total energy E_i of the ith particle in the sphere is defined as

$$E_i = \frac{mv_i^2}{2} - \sum_{j\neq i(r_j<R)}^{N_s} \frac{Gm^2}{\sqrt{r_{ij}^2 + r_0^2}}, \tag{5}$$

where E_i is rescaled using Eq. (3). Note that the particles outside the sphere can pass through the wall freely and, therefore, the system inside and outside the sphere evolves as microcanonical ensemble simulations; i.e., all particles inside and outside the sphere interact with each other during our evaporation process. If a particle reenters the sphere, we count it again as a particle inside the sphere. The properties in the sphere are computed including the reentering particle. We consider such a mass and energy loss in the container as a kind of evaporation process. We call this the "evaporation-collapse process" in the present study.

N is set to be 250, which is larger than 125 for the cold collapse process. This is because the number N_s of particles in the sphere decreases during the evaporation-collapse process. For the initial setup, we prepare the self-gravitating system at an approximate virial equilibrium state, using adiabatic walls [30]. To obtain the approximate virial equilibrium state, the microcanonical ensemble simulation is continued over 10 units of time. Based on the initial setup, a simulation of the evaporation-collapse process is carried out, using semipermeable walls. $\varepsilon_{\rm esc}$ and the initial total energy ε_0 are set to $\varepsilon_{\rm esc} = 0$ and $\varepsilon_0 = -0.3$, respectively. ($\varepsilon_0 = -0.3$ is slightly higher than the collapse energy, $\varepsilon_{\rm coll} \approx -0.339$. If the initial total energy is further higher, it is difficult to observe the evaporation-collapse process properly since most particles rapidly evaporate.) The simulation time for the evaporation-collapse process is set to 40 in our units.

To simulate the evaporation-collapse process, a couple of well-studied simple mechanisms are added to the cold collapse process. We expect that the evaporation-collapse process is difficult to predict theoretically, since both mass and energy vary simultaneously. Therefore, it is worthwhile to study this simple model numerically, in order to acquire a deeper understanding of nonequilibrium phenomena appearing in self-gravitating N-body systems.

C. Parameters for simulations

For velocity distributions in the sphere, we examine one-dimensional velocity distribution functions combining all-directional components of the velocity distribution [32]. The velocity distribution function $f(v)$ is first averaged over 30 simulations. After the ensemble average is obtained, velocity distribution functions for $t \leqslant 30$ and $t > 30$ are time-averaged over $\Delta t = 0.1$ and $\Delta t = 1$–2, respectively, to observe the distribution function more clearly. We have confirmed that the above operations do not greatly influence our main result.

Since the 1960s, several non-Gaussian velocity distribution functions have been suggested and examined for self-gravitating systems [20–23,27,31–33,54]. In those works, the q-Gaussian distribution based on Tsallis' statistics [4,20–22] was selected as a model to study whether the obtained distribution function is Gaussian. (Lynden-Bell's statistics [10], Renyi's statistics [16], Tsallis' statistics [17], etc., have been suggested for generalized statistics of the self-gravitating system.) In the present paper, the q-Gaussian distribution function is given by

$$f_q(v;q,A,B) = A\exp_q(-Bv^2), \tag{6}$$

where

$$\exp_q(-Bv^2) \equiv [1 - B(1-q)v^2]^{1/(1-q)} \tag{7}$$

and

$$\exp_1(-Bv^2) = \exp(-Bv^2). \tag{8}$$

q is the Tsallis entropic parameter. (A and B correspond to a normalization parameter and an inverse of temperature $1/2k_BT$, respectively [20,22]. The three parameters q, A, and B depend on time t. In the present study, we determine the parameters from the simulated velocity distribution, as described later.) If $q = 1$, the velocity distribution is Gaussian and Maxwell-Boltzmann. We determine q, minimizing the following function χ^2 [26]:

$$\chi^2(q,A,B) = \sum_{i=1}^{N_v} \left[\frac{f_{\rm sim}(v) - f_q(v;q,A,B)}{f_{\rm sim}(v)}\right]^2, \tag{9}$$

where $f_{\rm sim}(v)$ and N_v represent the simulated velocity distribution function at time t and the number for computing the summation, respectively. Note that N_v in Eq. (9) is set to 10–50, taking into account the range of the simulated velocity distribution function, as described in step I and step II. (Figure 2 shows typical simulated velocity distribution functions.)

In this study, we determine the three temporal parameters q, A, and B in Eq. (6) in the following steps [59]:

(I) We first assume a Gaussian distribution (i.e., $q = 1$) to determine A. By means of a quasi-Newton method, A and

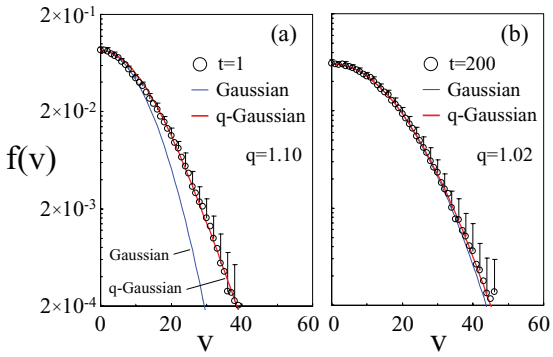

FIG. 2. (Color online) Velocity distribution functions of a cold collapse process for $\varepsilon = -1.0$. (a) $t = 1$. (b) $t = 200$. The open circles represent the simulated velocity distribution functions. The interval of the velocity is set to $\Delta v = 1$ in our units. The error bars indicate the 68% confidence level in terms of the normal error distribution (typical error bars are plotted). Note that the fitted Gaussian and q-Gaussian distributions are superposed. For step I, the Gaussian distributions are fitted by using only low-velocity particles, i.e., $v < 10$ (see the text for details).

B are computed, minimizing χ^2. In this step, we employ the simulation results only for low-velocity particles for $v < 10$. Accordingly, N_v in Eq. (9) is set to be 10 in this step.

(II) We determine q and B, assuming that the obtained A is fixed. In this step, we employ the simulation results for low- and high-velocity particles, to determine q and B minimizing χ^2. For example, in Fig. 2, the q-Gaussian distributions are fitted with the simulation results for $v < 40$; i.e., $N_v = 40$. [To set N_v, we monitor the temporal simulated velocity distribution function for $f(v) > 2 \times 10^{-4}$, as shown in Fig. 2. Therefore, in several cases, N_v is set to be different values; e.g., $N_v = 35$, 45, or 50.]

We have evaluated q through the above procedure and have confirmed that the determined parameters converge on nearly identical solutions and that B increases approximately linearly with the inverse of temperature, $1/T$. [The temperature T is given by $T = (2/3)\varepsilon_{\rm KE}$, assuming that the rescaled kinetic energy $\varepsilon_{\rm KE}$ corresponds to the temperature, as shown in Eq. (4).] In this paper, we have checked $f_{\rm sim}(v)$, the q-Gaussian distribution $f_q(v; q, A, B)$, and the function χ^2. Moreover, to observe the temporal goodness of fit, we have examined the normalized goodness of fit $\overline{\chi^2}$:

$$\overline{\chi^2} = \frac{\chi^2}{N_v}. \tag{10}$$

To obtain an overview of the velocity distributions from another viewpoint, we define the ratio of velocity moments, $v_{\rm m}(t)$, as

$$v_{\rm m}(t) = \frac{\langle v_i^2 \rangle^2}{\langle v_i^4 \rangle}, \tag{11}$$

where v_i is the speed of the ith particle in the sphere, and $\langle X \rangle$ represents the mean of X at time t [34,58]. If the speed distribution functions are Maxwell-Boltzmann and Gaussian, i.e., $f(v) = 4\pi v^2 (m/2\pi k_B T)^{3/2} \exp(-mv^2/2k_B T)$, $v_{\rm m}(t)$ approaches the specific value $v_{\rm mMB}$ of 0.6. In this study, the ratio of velocity moments is normalized as

$$V_{\rm M}(t) = \frac{v_{\rm m}(t)}{v_{\rm mMB}}. \tag{12}$$

Accordingly, the normalized ratio of velocity moments $V_{\rm M}(t)$ approaches 1 when the speed distribution is Gaussian. As mentioned above, the speed v_i of the ith particle in the sphere is employed to compute $v_{\rm m}(t)$, since the speed distributions are directly related to the velocity distributions. In this paper, we call $V_{\rm M}(t)$ the normalized ratio of velocity moments. We observe q and $V_{\rm M}(t)$ to discuss an overview of the velocity distributions. [The fluctuations of $V_{\rm M}(t)$ considered here are slightly smaller than those of $V'_{\rm M}(t)$ which is computed from the one-dimensional velocity of the particles inside the sphere. We have confirmed that a time-averaged $V_{\rm M}$ approximately agrees with a time-averaged $V'_{\rm M}$, when $V_{\rm M}(t)$ and $V'_{\rm M}(t)$ are time-averaged over $\Delta t = 0.1$.]

The virial ratio $\alpha(t)$ is defined as

$$\alpha(t) = \frac{2E_{\rm KE} - 4\pi R^3 P_{\rm wall}}{|E_{\rm PE}|}, \tag{13}$$

where $P_{\rm wall}$ represents the pressure on the container wall by the reflecting particles [29,30,34]. The pressure on the reflecting wall at time t can be evaluated as

$$P_{\rm wall}(t) = \frac{\sum_{\hat{t}=t-t''/2}^{\hat{t}=t+t''/2} 2m v_{\rm r}(\hat{t})}{4\pi R^2 t''} = \frac{\sum_{\hat{t}=t-t''/2}^{\hat{t}=t+t''/2} m v_{\rm r}(\hat{t})}{2\pi R^2 t''}, \tag{14}$$

where $v_{\rm r}(\hat{t})$ is the sum of the radial components of the velocities of all particles reflected by the wall, at each time step $\hat{t}$. In the present study, the interval t'' in Eq. (14) is set to be $t'' = 0.02$–0.20 in our units to reduce large fluctuations in the pressure [29,30]. The virial ratio is 1 if the system is in the virial equilibrium state with pure gravitational potentials. Note that the virial ratio in core-halo states with soft gravitational potentials is not 1, since particles in the core are well within the softening radius (i.e., the softening parameter r_0), unlike for pure gravitational potentials [34]. For example, the virial ratio defined by Eq. (13) is evaluated as 0.555, in the core-halo state with $\varepsilon = -0.339$ and $r_0 = 0.005$ [34].

During a collapse process of small N-body systems, it is difficult to observe density profiles because of strong fluctuations in the position of the high-density parts, even if the center of mass of the system of reference is considered [34]. Therefore, instead of the density profile, we examine the number N_c of core particles of a prescribed radius r_c [34]. According to Ref. [34], we count the number N_i of particles which are within r_c from the ith particle and find the particle which has the largest N_i. The prescribed radius r_c is set to be 0.01 [34]. We have confirmed that, except for an early relaxation process, the number N_c of core particles is not influenced much by the choice of a larger radius; e.g., $r_c = 0.02$. In our simulations, we generally did not observe a second-largest core containing more than two particles.

III. RESULTS

A. Cold collapse process

In this subsection, we examine a cold collapse process with constant mass and energy; i.e., we discuss the properties of the system enclosed in a spherical container with adiabatic walls. Figure 3 shows time evolutions of the properties of the cold collapse process for $\varepsilon = -0.6$, -0.8, -1.0, and -1.2. In this figure, the horizontal axis t is a logarithmic scale to observe evolutions of the system on time scales of the crossing, relaxation, and collapse times.

We first focus on the simulation results for $\varepsilon = -1.0$ as a typical result and discuss the influence of the total energy. As shown in Fig. 3(a), initially ($t \lessapprox 0.2$) the number N_c of core particles is approximately constant, because a collapse has not yet started. However, the temperature T significantly fluctuates, since the initial temperature is extremely low in strong nonequilibrium states due to our initial setup for the cold collapse. The period of the oscillations is approximately 0.2. (The period is likely related to the crossing time τ_c of the present system with $N = 125$ particles, $\tau_c \approx 0.2$, which is proportional to the period of plasma oscillations in a medium with charge concentration [29,34].) Of course, the crossing time discussed here likely depends on the total energy. That is, the higher the negative energy, the shorter the crossing time or the earlier the temperature increases.

Similarly, the virial ratio α for $\varepsilon = -1.0$ fluctuates initially, as shown in Fig. 3(b). However, α gradually approaches 1 for

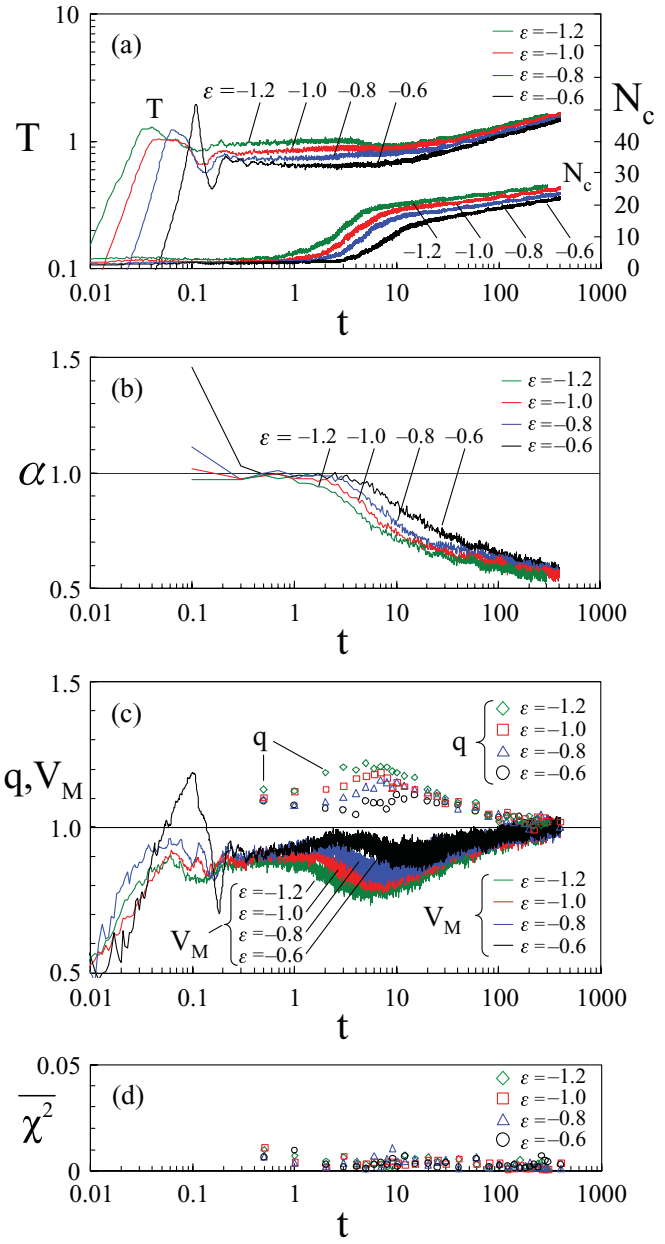

FIG. 3. (Color online) Time evolutions of the properties of the cold collapse process for various total energies ε. (a) Temperature T and number N_c of core particles. (b) Virial ratio α. (c) Normalized ratio of velocity moments $V_{\rm M}$ and Tsallis entropic parameter q. (d) Normalized goodness of fit $\overline{\chi^2}$. The horizontal axis t and the vertical axis for T are logarithmic scales. α starts from $t = 0.1$ ($=t''/2$), since the interval t'' in Eq. (14) is set to be $t'' = 0.2$ in our units. q is plotted from $t = 0.5$.

$0.5 \lessapprox t \lessapprox 1$. Therefore, the system is in an approximate virial equilibrium state or a quasiequilibrium state during this stage. However, after this stage ($t \gtrapprox 1$), N_c increases and α gradually deviates from 1 [Figs. 3(a) and 3(b)]. This suggests that a collapse should start from $t \approx 1$. (In this study, the Plummer softened potential is employed to simulate self-gravitating N-body systems. Therefore, the virial ratio in core-halo states deviates from 1, since the core particles are well within the softening radius.) As described in Ref. [34], the collapse starts immediately in the present small N-body system, since the total energy is set to be lower than the collapse energy, $\varepsilon_{\rm coll} \approx -0.339$. We expect that the system starts to deviate from the virial equilibrium state or the quasiequilibrium state, since the core starts to form. This deviation of α depends on the total energy; i.e., the higher the negative energy, the earlier the deviation starts. (Note that α for $\varepsilon = -1.2$ likely deviates from 1 even in the early stage, because of its higher negative energy.) Similarly, the higher the negative energy, the earlier the core starts to form [Fig. 3(a)].

For $t \gtrapprox 7$, the increase of N_c with $\varepsilon = -1.0$ tends to be slower than that of the early stage [Fig. 3(a)] and α gradually approaches a certain value [Fig. 3(b)]. Therefore, we expect that the system should gradually approach a core-halo state, after undergoing the virial equilibrium state. Interestingly, T starts to increase after a delay of several time units ($t \gtrapprox 10$). In other words, T increases clearly, after the core forms sufficiently. This indicates that the density evolution due to a growth of the core plays a leading role in the collapse process, as has been pointed out by Ispolatov and Karttunen [34]. It should be noted that our system has not yet approached a complete core-halo state, since the simulated temperature is lower than the predicted value based on mean-field theory [34]. In this paper, we do not discuss the system in the complete core-halo state. (For example, in the complete core-halo state, the predicted temperature for $\varepsilon = -1.0$ is approximately evaluated as 2.3 from a phase diagram in Ref. [34].)

As shown in Fig. 3(a), all the slopes of N_c are similar after a rapid increase of N_c ($t \gtrapprox 10$); i.e., N_c increases approximately logarithmically with time. (We call this a start time of logarithmic increase of N_c.) In particular, since T increases approximately linearly with t in the logarithmic-scale plot, the time evolution of the temperature may be related to a power law, $T \propto t^{\delta}$ ($\delta \approx 0.2$), in this stage. We expect that collisions tend to be further dominant in this stage, since $t \gtrapprox 10$ is sufficiently longer than the relaxation time, $\tau_r \approx 0.5$.

In our cold-collapse process, the number N of particles is set to be 125. We can expect that the complete collapse time gradually increases with increasing N, in our units [34]. (In Ref. [34], the complete collapse time has been examined for systems consisting of 125–500 particles.) Similarly, the start time of logarithmic increase of N_c mentioned above is expected to increase with N. Therefore, we have examined the cold collapse process for the system consisting of 250 particles for $\varepsilon = -1.0$, to observe an overview of the effect of the size of the system (Appendix). Consequently, the start time of logarithmic increase of N_c likely depends on N; i.e., the start time for $N = 250$ is slightly later than the start time for $N = 125$. Moreover, the cold collapse process for $N = 250$ is consistent with the process for $N = 125$ discussed in this subsection. The details are summarized in the Appendix. (Note that larger N-body systems should be simulated to study the effect of the size of the system in more detail. However, longer computational time and smaller time steps are required to maintain the accuracy of the collapse simulation for the larger systems. In the present paper, we focus on the small N-body systems.)

To study the influence of the total energy more clearly, we observe the dependence of T, α, and N_c on the total energy, as shown in Fig. 4. In this figure, as a typical result, the properties at time $t = 30$ are plotted from Figs. 3(a) and 3(b). [Figure 3(c)

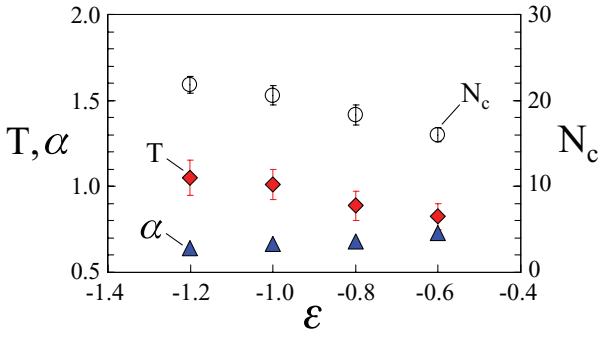

FIG. 4. (Color online) Dependence of T, α, and N_c on the total energy ε at $t = 30$. The plotted α is the average of the values for $t = 29.9$ and $t = 30.1$.

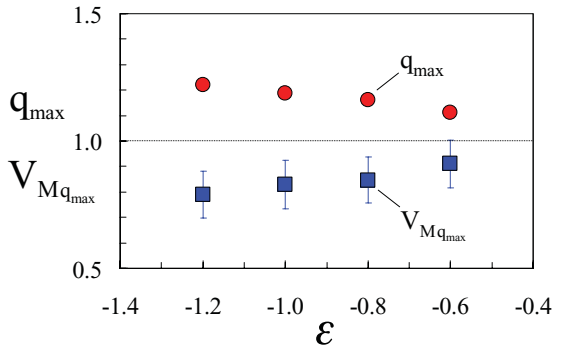

FIG. 5. (Color online) Dependence of $q_{\max}$ and $V_{\mathrm{M}q_{\max}}$ on the total energy ε. The maximum Tsallis entropic parameter $q_{\max}$ for each total energy is plotted from Fig. 3(c). Note that $V_{\mathrm{M}q_{\max}}$ represents the normalized ratio of velocity moments required for $q_{\max}$. $V_{\mathrm{M}q_{\max}}$ is averaged over the same time interval for $f_{\mathrm{sim}}(v)$ to determine q.

is discussed in the next paragraph.] As shown in Fig. 4, T and N_c increase with increasing negative total energy, $-\varepsilon$ (or with decreasing total energy, ε). In contrast, α decreases with the negative total energy. This indicates that the core forms easier for higher negative energy and, therefore, the system further deviates from the virial equilibrium state.

We now examine time evolutions of the normalized ratio of velocity moments V_{M} and the Tsallis entropic parameter q, to discuss the velocity distributions. (Note that V_{M} is computed from the speed of particles, as described in Sec. II C.) As shown in Fig. 3(c), V_{M} and q deviate from 1 for $t \lessapprox 1$. Therefore, the velocity distribution is non-Gaussian in a quasiequilibrium state, since ε is lower than $\varepsilon_{\mathrm{coll}} \approx -0.339$. For example, as shown in Fig. 2(a), the velocity distribution for $\varepsilon = -1.0$ is well fitted with the q-Gaussian distribution with $q \approx 1.1$ in the early relaxation process ($t = 1$). The q-Gaussian distribution is likely well fitted with the simulation results through the cold collapse process, since the normalized goodness of fit $\overline{\chi^2}$ defined by Eq. (10) is sufficiently small as shown in Fig. 3(d). (In Sec. III B, we will discuss this in detail.) From Fig. 3(c), we found that V_{M} and q with $\varepsilon = -1.0$ further deviate from 1 for $1 \lessapprox t \lessapprox 7$. That is, the velocity distribution further deviates from the Gaussian distribution, when the core forms rapidly. The deviation of q and V_{M} from 1 depends on the total energy.

To examine this deviation more closely, we plot the maximum Tsallis entropic parameter $q_{\max}$ and the normalized ratio $V_{\mathrm{M}q_{\max}}$ of velocity moments required for $q_{\max}$, as a function of ε. As shown in Fig. 5, $q_{\max}$ and $V_{\mathrm{M}q_{\max}}$ further deviate from 1 with increasing negative total energy, $-\varepsilon$. In other words, the greater the negative energy, the farther the deviation from a Gaussian distribution.

We further observe the time evolutions of q and V_{M} for $\varepsilon = -1.0$. As shown in Fig. 3(c), for $t \gtrapprox 7$, V_{M} starts to increase while q starts to decrease and they gradually approach 1. This indicates that the velocity distribution evolves from non-Gaussian to an approximate Gaussian distribution after the core forms sufficiently. For $t \gtrapprox 200$, the velocity distribution for $\varepsilon = -1.0$ approaches a Gaussian-like distribution, since V_{M} and q are approximately 1. In fact, as shown in Fig. 2(b), q at time $t = 200$ is close to 1. (The Gaussian distribution at $t = 200$ is well fitted with the simulation result, although only low-velocity particles are employed for the fitting.) (Such a variation in velocity distributions is also affected by a temperature change during the collapse process; i.e., the velocity distribution should deviate from the original distribution due to the temperature change. If the original velocity distribution is Gaussian and if the negative energy of the system is not high, the deviation from Gaussian is expected to decrease immediately, following the temperature change.)

In the present cold collapse simulation, the velocity distribution likely approaches the approximate Gaussian distribution for $t \gtrapprox 200$–300; that is, the velocity distribution relaxes faster than other thermodynamic properties, e.g., temperature T. Therefore, the velocity distribution evolves from a non-Gaussian distribution ($q = q_1 > 1$) through a higher non-Gaussian distribution ($q > q_1$; i.e., the velocity distribution further deviates from Gaussian) to a Gaussian-like distribution ($q \approx 1$), in the long-term evolution of the cold collapse process, where q_1 represents q for quasiequilibrium states. Of course, it takes much longer for the velocity distribution to evolve from the higher non-Gaussian distribution to the Gaussian-like distribution. As shown in Fig. 3(b), the virial ratio should evolve monotonically from the value for a quasiequilibrium state to that for a core-halo state. However, we found that the velocity distribution does not evolve monotonically, unlike the virial ratio. In other words, the velocity distribution undergoes higher non-Gaussian distributions, especially when the core forms rapidly in an early collapse process. We have clearly shown that such a transition of the velocity distribution based not only on q but also on V_{M}.

As discussed above, it takes a longer time for the velocity distribution to approach the Gaussian distribution in our cold collapse process. However, in plasma physics, it is well known that the velocity distributions in a Coulomb system approach the Gaussian distributions in a short time. For example, it has been reported that the velocity distribution remains Gaussian during collapse simulations, because of the fast velocity relaxation [34]. In Ref. [34], the initial velocity distribution is Gaussian, and the total energy for a collapse is typically set to be $\varepsilon = -0.3 \sim -0.5$. In contrast, in our cold collapse simulation, the initial velocity distribution is a delta-function-like distribution with negligible small values, and the total energy is set to be $\varepsilon = -0.6$, -0.8, -1.0, and -1.2, which are relatively lower than the collapse energy $\varepsilon_{\mathrm{coll}} = -0.339$. (This is because we would like to observe variations in velocity distributions clearly.) In fact, we have confirmed that, for $\varepsilon = -0.6$, the velocity distribution further

deviates from Gaussian after a collapse starts, even if the initial velocity distribution is set to be a Gaussian-like distribution [60]. Therefore, the deviation from Gaussian discussed here is likely influenced by higher negative energy. We can confirm this from Fig. 5; i.e., $q_{\max}$ and $V_{\mathrm{M}q_{\max}}$ further approach 1 with increasing ε. Moreover, we have checked that, for $\varepsilon = -0.2$, the velocity distribution does not likely deviate from a Gaussian-like distribution except in an early relaxation process, even if the initial velocity distribution is set to be a delta-function-like distribution [61]. Note that further research is required to examine the velocity relaxation in more detail.

In this study, q is obtained from fitting with the simulated velocity distributions. Therefore, we should not deny a phenomenological aspect of our study. However, we can expect a good correlation between V_{M} and q, from Fig. 3(c) or Fig. 5. That is, the increase of q and the decrease of V_{M} are consistent with each other, and vice versa. We will discuss this correlation in the next subsection.

B. Evaporation-collapse process

To examine mass and energy loss in a collapse, we consider an "evaporation-collapse process" in this subsection. In the evaporation-collapse process, a particle outside the sphere can return into the sphere freely. All particles inside and outside the sphere interact with each other during the evaporation-collapse process, because of long-range potentials. If a particle reenters the sphere, we count it again as a particle inside the sphere. The properties in the sphere are computed including the reentering particle. However, most particles outside the sphere do not likely return into the sphere again. The model considered here is one of the possible models to simulate the evaporation-collapse process. Since the number N_s of particles in the sphere is initially set to be 250, the crossing and relaxation times are evaluated as $\tau_c \approx 0.1$ and $\tau_r \approx 0.6$, respectively. In the following, we discuss the properties of the open system in the sphere. Note that the simulation results of the evaporation-collapse process are slightly complicated to interpret, since mass and energy vary simultaneously.

We first observe the time evolutions of the properties of the evaporation-collapse process with mass and energy loss. As shown in Fig. 6(a), N_s decreases from the initial value of 250, since high-energy particles escape from the sphere. For $t \lessapprox 0.6$, the virial ratio α deviates from 1 because of our initial setup [Fig. 6(b)]. However, for $0.6 \lessapprox t \lessapprox 7$, α is approximately 1 and, therefore, we expect that the system is in an approximate virial equilibrium state. In this stage, the temperature T and the negative total energy $-\varepsilon$ in the sphere gradually increase [Fig. 6(a)]. That is, a negative specific heat occurs in the evaporation-collapse process. However, for $t \gtrapprox 7$, α gradually deviates from 1 [Fig. 6(b)]. This indicates that the system in the sphere gradually deviates from the virial equilibrium state, as for the cold collapse process. In this stage, N_s decreases rapidly, as shown in Fig. 6(a). Moreover, T, $-\varepsilon$, and the number N_c of core particles increase rapidly.

As discussed in Ref. [30], we expect that the deviation of α from 1 is related to a deviation from an ε-T curve for stellar polytropes. To examine this, we plot the dependence of the properties on the total energy ε in the early stage ($t \approx 0$–10). In Fig. 7, the ε-T curve of Emden solutions with $n = 9$ and

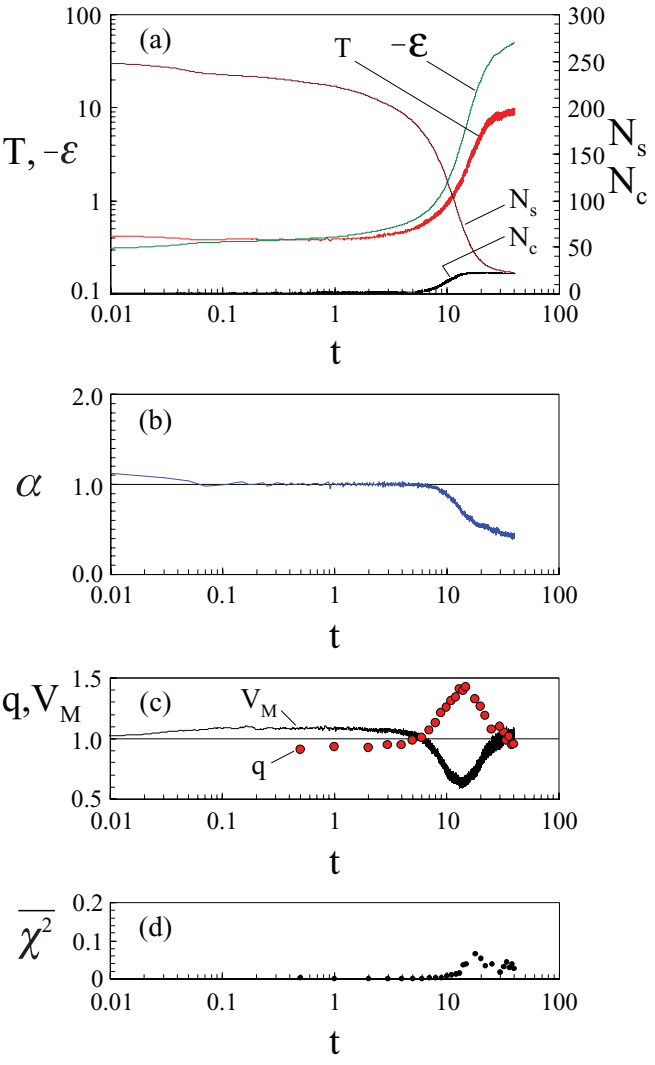

FIG. 6. (Color online) Time evolutions of the properties of the evaporation-collapse process with mass and energy loss. (a) Temperature T, negative total energy $-\varepsilon$, number N_c of core particles, and number N_s of particles in the sphere. (b) Virial ratio α. (c) Normalized ratio of velocity moments V_{M} and Tsallis entropic parameter q. (d) Normalized goodness of fit $\overline{\chi^2}$. For α, the interval t'' in Eq. (14) is set to be $t'' = 0.02$ in our units. The initial $q(0)$ is not shown due to the logarithmic time scale.

$n = \infty$ are also plotted for stellar polytropes, where n represents the polytrope index [30]. (The polytropic relation can be given as $P \propto \rho^{1+1/n}$. The polytrope index of $n = \infty$ corresponds to isothermal spheres. In Ref. [30], the simulated ε-T curve for an evaporation process agrees well with the curve for the stellar polytrope with $n \sim 9$.) In this figure, the simulated system evolves as indicated by the arrow, since the simulation starts from the initial total energy of -0.3.

As shown in Fig. 7(a), for $-0.7 \lessapprox \varepsilon < -0.3$, α is approximately 1 and T agrees well with that for the stellar polytrope with $n = 9$. However, for $\varepsilon \lessapprox -0.7$, α gradually deviates from 1. As expected, α starts to deviate from 1 when T starts to deviate from that for the stellar polytrope with $n = 9$. Moreover, we found that N_c increases for $\varepsilon \lessapprox -0.6$. That is, after the core starts to form, the system deviates from

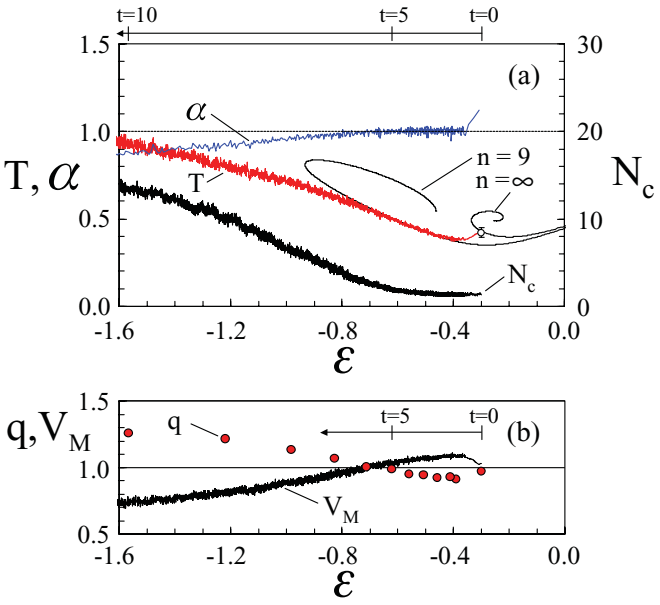

FIG. 7. (Color online) Dependence of the properties on the total energy ε in the early evaporation-collapse process for $t \approx 0$–10. (a) Temperature T, virial ratio α, and number N_c of core particles. (b) Normalized ratio of velocity moments $V_{\rm M}$ and Tsallis entropic parameter q. The simulated system evolves as indicated by the arrow with time t, from $\varepsilon = -0.3$. In (a), the initial temperature is represented by the open circle. The ε-T curves of Emden solutions with $n = 9$ and $n = \infty$ are indicated for the stellar polytrope [30]. The horizontal line corresponds to the virial equilibrium state, i.e., $\alpha = 1$. In (b), q for $t = 0, 0.5, 1, 2, \ldots, 9$, and 10 evolves from right to left.

both the virial equilibrium state and the stellar polytrope. The deviation of α from 1 is consistent with the formation of the core, since many core-particles are well within the softening radius of the Plummer softened potential [34]. As shown in Fig. 7(b), initially, i.e., at $\varepsilon = -0.3$, the normalized ratio of velocity moments $V_{\rm M}$ and Tsallis entropic parameter q are approximately 1. Therefore, the initial velocity distribution is approximately Gaussian, since the initial total energy ε_0 of -0.3 is slightly higher than the collapse energy $\varepsilon_{\rm coll}$ of -0.339. However, in an early stage, i.e., for $-0.7 \lessapprox \varepsilon < -0.3$, $V_{\rm M}$ and q deviate from 1, while the virial ratio is approximately 1. In other words, the velocity distribution is non-Gaussian, while the system is in the approximate virial equilibrium state. It should be noted that q is less than 1 and $V_{\rm M}$ is larger than 1, unlike for the cold collapse process. This suggests that many high-velocity particles with positive energy escape from the sphere during the early evaporation process. Accordingly, in principle, the velocity distribution in this stage deviates from the Gaussian distribution, since the velocity distribution considered here is computed from velocity of the particles inside the sphere. However, for $\varepsilon \lessapprox -0.7$, q and $V_{\rm M}$ gradually tend to be larger and smaller than 1, respectively, as for the cold collapse process. After the early evaporation process, the deviation of q and $V_{\rm M}$ from 1 does not depend much on the escape of the positive-energy particles. Therefore, in this stage, the deviation from the Gaussian distribution is likely related to the formation of the core.

We now further discuss the time evolutions of the properties in the evaporation-collapse process. As shown in Fig. 6(a), after the core starts to form, T increases rapidly, as for the cold collapse process. However, the delay of the temperature increase is not so clear, since in the evaporation-collapse process, T depends not only on kinetic energy but also on N_s. The growth of the core stops at $t \approx 20$ and, finally, N_c is approximately equal to N_s. On the other hand, the virial ratio slowly decreases and gradually approaches a value corresponding to a core-halo state for $t \gtrapprox 15$ [Fig. 6(b)]. Note that the system has not yet approached the complete core-halo state in the present simulation.

To examine the velocity distributions, we observe $V_{\rm M}$ and q. As shown in Figs. 6(c) and 7(b), the initial velocity distribution is approximately Gaussian due to our initial setup [the initial $q(0)$ is not shown in Fig. 6(c), due to the logarithmic time scale]. However, for $0 < t \lessapprox 4$, $V_{\rm M}$ and q deviate from 1. In this stage, q is less than 1 while $V_{\rm M}$ is larger than 1, since many high-velocity particles with positive energy escape from the sphere, as mentioned previously. For $7 \lessapprox t \lessapprox 15$, $V_{\rm M}$ and q further deviate from 1, because of a rapid growth of the core. However, for $t \gtrapprox 15$, $V_{\rm M}$ increases while q decreases, and they gradually approach 1. Accordingly, the velocity distribution evolves from a non-Gaussian distribution ($q = q_1 \neq 1$) through a higher non-Gaussian distribution ($q > q_1$; i.e., the velocity distribution further deviates from Gaussian) to an approximate Gaussian distribution ($q \approx 1$), as for the cold collapse process. This suggests that we can evaluate the ages of stellar clusters from their velocity distributions. In fact, Carvalho *et al.* have found that the q parameter in the Tsallis distribution depends on the ages of open stellar clusters, using observed radial velocities of the clusters [33].

Interestingly, for $t \gtrapprox 25$, although the velocity distribution is approximately Gaussian, a negative specific heat occurs; i.e., $-\varepsilon$ increases with T, as shown in Fig. 6(a). Of course, the thermodynamic properties considered here, i.e., ε and T, depend on N_s. Accordingly, the system in this stage may not be suitable for discussing the thermodynamic properties, since N_s is small, $\sim$20.

In the present study, we determine the Tsallis entropic parameter $q(t)$, minimizing the function χ^2. To examine the difference from a q-Gaussian distribution, we observe the normalized goodness of the fit $\overline{\chi^2}$ defined by Eq. (10). This parameter indicates that the greater $\overline{\chi^2}$, the worse the fit. As shown in Fig. 6(d), $\overline{\chi^2}$ is large especially for $15 \lessapprox t \lessapprox 25$. Therefore, after q starts to decrease (or when a growth of the core begins to slow down), the q-Gaussian distribution is not well fitted with the simulated velocity distribution. This is because N_s tends to be small but also because the simulated velocity distribution has an apparent cusp profile in the low-velocity regions (such a cusp velocity profile has been observed in a collapse process; e.g., see Ref. [32]). For $t \gtrapprox 25$, $\overline{\chi^2}$ is slightly large due to statistical errors of high-velocity particles, since N_s is small. However, we did not observe the apparent cusp profile for $t \gtrapprox 25$. We have confirmed that the q-Gaussian distribution is well fitted with the simulated velocity distribution, except for $15 \lessapprox t \lessapprox 25$. In the cold collapse process, the q-Gaussian distribution is well fitted with the simulated velocity distributions, since the cusp profile does not clearly appear and N_s is fixed. It should be noted that the q-Gaussian distribution discussed here is

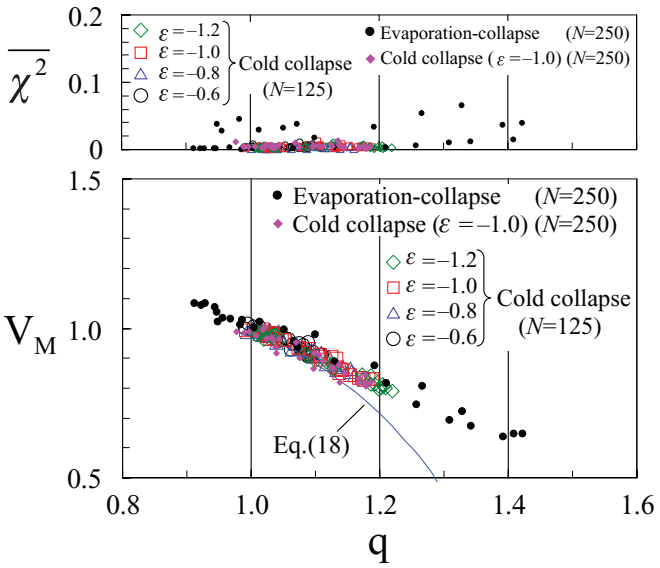

FIG. 8. (Color online) Dependence of the normalized ratio of velocity moments V_M on the Tsallis entropic parameter q. Top: Normalized goodness of fit $\overline{\chi^2}$. Bottom: Normalized ratio of velocity moments V_M. V_M is averaged over the same time interval for $f_{sim}(v)$ to determine q. The solid line represents $V'_{Mex}(q)$ defined by Eq. (18) based on one-dimensional velocity distributions (while the simulated V_M is computed from the speed of the particles inside the sphere). Note that the pink diamonds (the closed diamonds) represent the cold collapse process of the system with $N = 250$ particles discussed in the Appendix.

selected as a possible model, to examine whether the simulated velocity distribution is Gaussian. [As mentioned above, the q-Gaussian distribution is not well fitted with the simulated velocity distribution when a higher non-Gaussian distribution appears. However, we can confirm that the simulated velocity distribution further deviates from Gaussian in this stage, since V_M further deviates from 1, as shown in Fig. 6(c).]

From Figs. 3(c) and 6(c), we expect that the correlation between V_M and q for the evaporation-collapse process agrees well with that for the cold collapse process. Therefore, to examine this correlation more closely, we plot the relationship between q and V_M, using all the results discussed in this paper. As shown in Fig. 8, the relationship between q and V_M is on a common curve. This indicates a good correlation between q and V_M. We found that both q and V_M are suitable for observing the long-term evolution of velocity distributions. The good correlation suggests that the q-Gaussian distribution is well fitted with the simulated velocity distribution in the present collapse process. We can confirm this from Fig. 8, since $\overline{\chi^2}$ is sufficiently small except for several results of the evaporation-collapse process. Of course, we should not deny a phenomenological aspect of our study, since q is obtained from fitting with the simulated velocity distribution. However, our simulation results can help to understand nonequilibrium phenomena appearing in self-gravitating N-body systems.

In our simulations, q is computed from the velocity distribution, while V_M is computed from the speed of the particles inside the sphere, as described in Sec. II C. However, if an alternative normalized ratio of velocity moments V'_M was computed from the one-dimensional velocity of the particles inside the sphere, we would directly compare between the simulated relation of V'_M to q and an exact relation of V'_{Mex} to q. For example, from Eqs. (6) and (7), the q-Gaussian distribution function is rewritten as

$$f_q(v) = A[1 + B(q-1)v^2]^{1/(1-q)}. \tag{15}$$

The mean value of squares of the velocity $\langle v^2 \rangle$ can be calculated as

$$\langle v^2 \rangle = \frac{\int v^2 f_q(v) dv}{\int f_q(v) dv}, \tag{16}$$

where $\int v^2 f_q(v) dv$ is divided by $\int f_q(v) dv$ (=1), according to a definition of the generalized nth moment [4]. Similarly, $\langle v^4 \rangle$ is given as

$$\langle v^4 \rangle = \frac{\int v^4 f_q(v) dv}{\int f_q(v) dv}. \tag{17}$$

Therefore, substituting Eq. (15) into Eqs. (16) and (17), by making the change of variables, i.e., $u = [B(q-1)]^{1/2} v$, the exact relation $V'_{Mex}(q)$ (for $q > 1$) is evaluated as

$$V'_{Mex}(q) = \frac{v'_m}{v'_{mMB}} = \frac{\langle v^2 \rangle^2 / \langle v^4 \rangle}{v'_{mMB}} = \frac{M_2^2 / M_4 / M_0}{v'_{mMB}}, \tag{18}$$

where

$$M_n = \int_0^\infty \frac{u^n}{(1+u^2)^{1/(q-1)}} du. \tag{19}$$

v'_{mMB} is the specific value of 1/3, for the Maxwell-Boltzmann velocity distribution. Of course, $V'_{Mex}(q)$ is different from V_M, since $V'_{Mex}(q)$ is calculated from the velocity (while V_M is computed from the speed) [62]. However, we have checked that a time-averaged V_M considered here approximately agrees with a time-averaged V'_M, as mentioned previously. Therefore, we attempt to compare between the exact relation $V'_{Mex}(q)$ and the simulated relation of V_M to q. For this purpose, $V'_{Mex}(q)$ defined by Eq. (18) is plotted as the solid line, as shown in Fig. 8. For $q \lessapprox 1.1$, the simulated relation of V_M to q likely agrees well with $V'_{Mex}(q)$. In contrast, for $q \gtrapprox 1.1$, the simulation results gradually deviate from $V'_{Mex}(q)$. The deviation may suggest that, the greater q, the worse the fit. In other words, the velocity distribution may vary from a q-Gaussian distribution to other non-Gaussian distributions, for $q \gtrapprox 1.1$. However, as shown in Fig. 8, the simulated V_M and the exact relation $V'_{Mex}(q)$ decrease with increasing q. Accordingly, our simulation results are consistent with the exact relation.

We have so far focused on velocity distributions in the collapse process. Finally, we examine the energy distributions and the density-velocity correlations in the collapse process. To this end, the energy distribution function $f(E_i)$ in the sphere is defined as $f(E_i) = N(E_i)/N_s$. Note that $N(E_i)$ is calculated from the number of particles with energy E_i between $E_i - dE_i$ and $E_i + dE_i$ [1,63,64], where E_i is the total energy of the ith particle in the sphere, as given by Eq. (5). $f(E_i)$ is averaged over 30 simulations and over $\Delta t = 0.1$–2, as for the velocity distribution functions $f(v)$. In this study, we examine $f(E_i)$ based on the non-rescaled energy E_i, since $f(E_i)$ is suitable for discussing our simulation results.

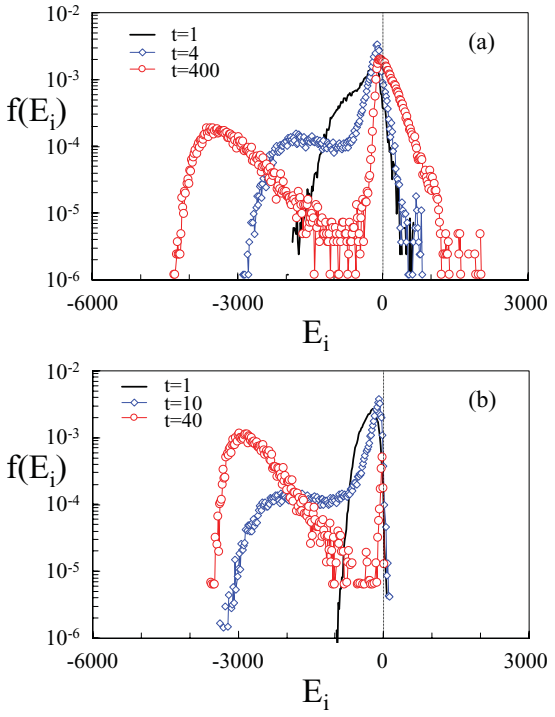

FIG. 9. (Color online) Temporal energy distribution functions $f(E_i)$. (a) Cold collapse process with $\varepsilon = -1.0$ for $t = 1$, 4, and 400 (the final time). (b) Evaporation-collapse process for $t = 1$, 10, and 40 (the final time).

As a typical result, we observe temporal energy distributions of the cold collapse process for $\varepsilon = -1.0$. As shown in Fig. 9(a), most of the particles are close to $E_i \sim 0$, in quasiequilibrium states ($t = 1$). However, high-negative-energy particles gradually appear during growth of the core, e.g., from $t = 4$ to $t = 400$. The high-negative-energy particles correspond to the core particles. In our cold collapse process, positive-energy particles exist in the sphere, since the particles cannot escape from the sphere due to adiabatic walls. Therefore, in the dynamical evolution of the system, the positive-energy particles gradually increase, while the core particles gradually tend to have higher negative energy. In contrast, in the evaporation-collapse process, positive-energy particles can escape from the sphere because of semipermeable reflecting walls. Accordingly, in principle, only negative-energy particles exist in the sphere, as shown in Fig. 9(b). The energy distribution for $t = 1$ is consistent with the results discussed in Refs. [63,64]. However, after the core starts to form, high-negative-energy particles gradually appear, e.g., from $t = 10$ to $t = 40$, as for the cold collapse process. This indicates that the growth of the core in each collapse process is consistent. However, at the final time, the energy distributions are clearly different from each other, although the velocity distributions of the two collapse processes are Gaussian-like.

The energy distributions discussed in Fig. 9 are related to density-velocity correlations. Therefore, we observe an overview of the density-velocity correlation, through a shell-averaged density and a shell-averaged velocity speed [29]. To calculate the shell-averaged values, we consider the following imaginary shells, according to Ref. [29]. In the spherical container of radius $R = 1$, the container is divided into 10 spherical shells in the radial direction r. The distance between the inner and outer shells is set to be $\Delta r = 0.1$. The origin of r is set to be the center of gravity. That is, to calculate the shell-averaged values, we consider the imaginary spherical shells which are fixed at the center of gravity. The radius $\Delta r = 0.1$ of the innermost shell is 10 times larger than the prescribed radius $r_c = 0.01$ (i.e., the criteria of the core) which should be larger than the core radius. Therefore, the shell-averaged density of the core-region should be at least 10^3 times smaller than the exact core density. (The shell-averaged density of the core region is significantly smaller than the exact core density, when the core forms. However, we can observe an overview of the density-velocity correlation, through the shell-averaged values.) In the evaporation-collapse process, we calculate the center of gravity using the particles inside the real spherical container with semipermeable reflecting walls. Note that the shell-averaged velocity considered here is the shell-averaged velocity speed V [29].

The temporal density-velocity correlations are shown in Fig. 10. We first observe the density-velocity correlations of the cold collapse process for $\varepsilon = -1.0$. As shown in Fig. 10(a), the velocity increases with density in quasiequilibrium states ($t = 1$) and early collapse processes ($t = 4$). The velocity increases as time progresses, since the core gradually forms (i.e., the density increases). This is consistent with the fact that high-negative-energy particles gradually appear, as discussed

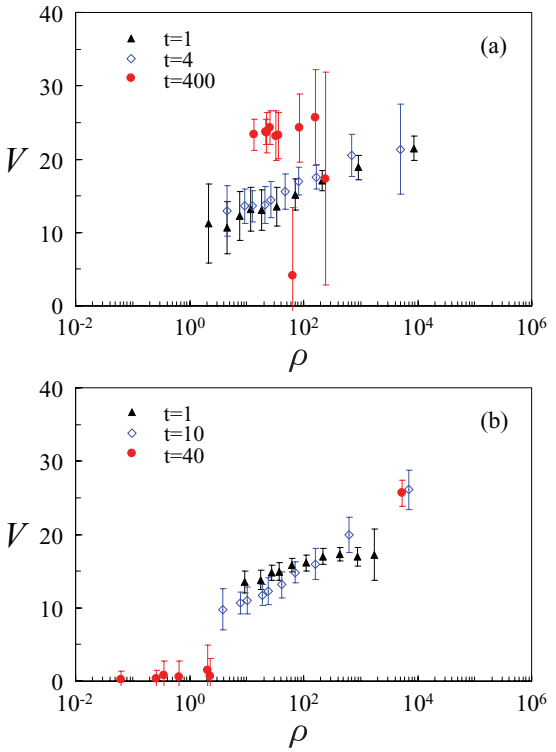

FIG. 10. (Color online) Dependence of the shell-averaged velocity speed on the shell-averaged density. (a) Cold collapse process with $\varepsilon = -1.0$ for $t = 1$, 4, and 400 (the final time). (b) Evaporation-collapse process for $t = 1$, 10, and 40 (the final time). The shell-averaged density of the core region should be at least 10^3 times smaller than the exact core density, when the core forms.

in Fig. 9(a). However, the density-velocity correlation is not clear at the final time ($t = 400$), although the velocity likely increases with density [Fig. 10(a)]. This is because we observe the shell-averaged values based on the center of gravity, when the position of the high-density parts fluctuates strongly [34]. In other words, the center of gravity is different from the position of the high-density parts, since many positive-energy particles exist in the sphere due to adiabatic walls for the cold collapse process [Fig. 9(a)].

In the evaporation-collapse process [Fig. 10(b)], the velocity increases with density, as for the cold collapse process. We found that high-density and high-velocity plots ($\rho \sim 10^4$) gradually appear, e.g., from $t = 10$ to $t = 40$, since the core starts to form. Of course, the shell-averaged density in this figure is significantly lower than the exact core density. However, the velocity in higher-density regions is higher than the velocity in lower-density regions. This suggests that the density-velocity correlation is clearly demonstrated in the evaporation-collapse process. In particular, the velocity gradient for $t = 10$ is likely higher than the gradient for $t = 1$; i.e., the velocity gradient increases as time progresses. In the present study, the kinetic energy corresponds to temperature and, therefore, the increase of the velocity gradient is likely related to a gravothermal instability derived from negative specific heat. An alternative simple interpretation is that positive-energy particles with high velocity in outer low-density regions escape from the sphere, through the evaporation-collapse process.

As shown in Fig. 10(b), a high-density and high-velocity plot ($\rho \sim 10^4$) clearly appears at the final time ($t = 40$). The high-density and high-velocity plot corresponds to the high-negative-energy particles discussed in Fig. 9(b). In contrast, at the final time ($t = 40$), the low-density and low-velocity plots ($\rho < 10^1$) in Fig. 10(b) likely correspond to particles in halo regions close to $E_i \sim 0$ in Fig. 9(b). We found that the density-velocity correlation is consistent with the energy distribution, through this overview based on the shell-averaged values.

IV. CONCLUSIONS

To clarify the velocity distributions and thermodynamic properties in self-gravitating N-body systems, we have numerically examined long-term evolution of those systems, from an early relaxation to a collapse. In the present study, we have considered two collapse processes: (1) a cold collapse process under a restriction of constant mass and energy and (2) an evaporation-collapse process with mass and energy loss. To examine the two processes, we have employed typical small N-body systems of 125–250 particles, through the Plummer softened potential.

It is shown that the q-Gaussian distributions based on the Tsallis entropy are well fitted with most simulated velocity distributions, except for several results of the evaporation-collapse process, especially except for $q \gtrapprox 1.1$. We found a good correlation between the Tsallis entropic parameter q and the normalized ratio of velocity moments $V_{\rm M}$. Moreover, the simulated relation of $V_{\rm M}$ to q is consistent with the exact relation $V'_{\rm Mex}(q)$. That is, q and $V_{\rm M}$ are suitable for observing the evolution of velocity distributions. In a quasiequilibrium state or an early relaxation process, the velocity distribution is non-Gaussian, when the total energy is lower than the collapse energy. Even if the initial velocity distribution is Gaussian, the velocity distribution rapidly deviates from a Gaussian distribution since the total energy decreases in the evaporation-collapse process. In dynamical evolutions of the system, the velocity distribution further deviates from the Gaussian distribution, especially in an early collapse process, i.e., when the core forms rapidly. However, after the core forms sufficiently, the velocity distribution gradually approaches an approximate Gaussian distribution. In this stage, the temperature for the cold collapse process increases rapidly, as if it obeyed a power law. We also found that a negative specific heat occurs in the evaporation-collapse process, even if the velocity distribution is Gaussian-like. In the evaporation-collapse process, the negative specific heat

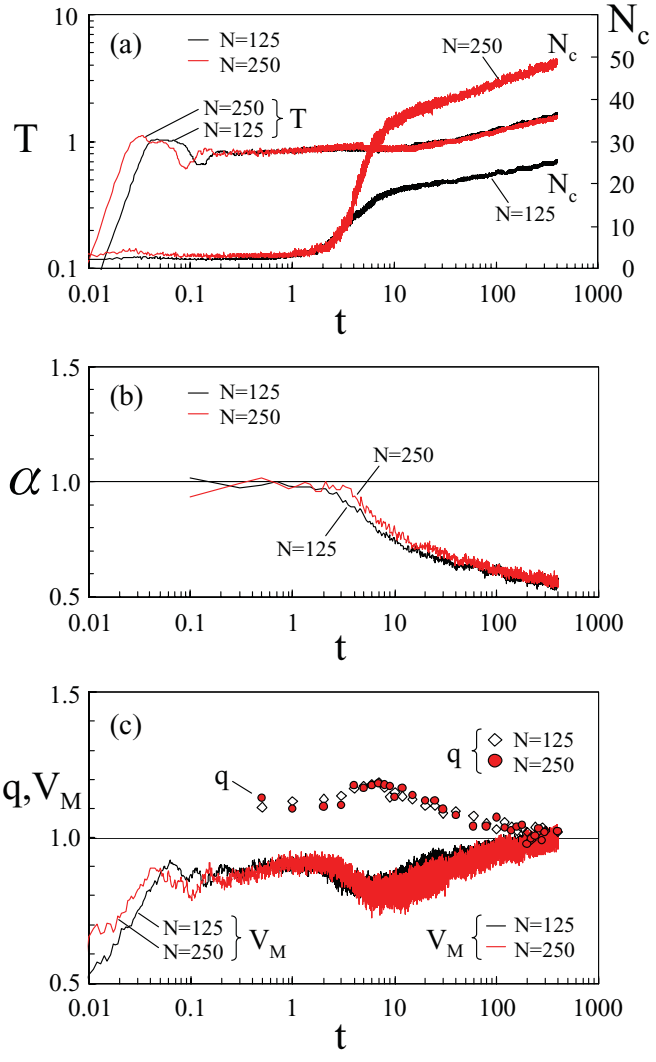

FIG. 11. (Color online) Time evolutions of the properties of the cold collapse process for $\varepsilon = -1.0$ with $N = 125$ and $N = 250$. (a) Temperature T and number N_c of core particles. (b) Virial ratio α. (c) Normalized ratio of velocity moments $V_{\rm M}$ and Tsallis entropic parameter q. The results for $N = 125$ are plotted from Fig. 3. See the caption of Fig. 3.

may be related to an increase of the velocity gradient observed in density-velocity correlations.

In our collapse processes, it is clearly shown that the velocity distribution evolves from a non-Gaussian distribution ($q = q_1 > 1$ or $\neq 1$) through a higher non-Gaussian distribution ($q > q_1$) to an approximate Gaussian distribution ($q \approx 1$). This suggests that observations of the velocity distribution should help to evaluate the ages of stellar clusters. Through the virial ratio, we usually expect that the system should monotonically evolve from a quasiequilibrium state in a collisionless stage to a core-halo state in a collisional stage. However, while the virial ratio decreases monotonically, the velocity distribution undergoes higher non-Gaussian distributions especially when the core forms rapidly in an early collapse process. The velocity distribution evolves dramatically in long-term evolutions of gravity-dominated systems, although the velocity distribution should finally approach a Gaussian-like distribution. The present study has revealed the evolution of self-gravitating N-body systems and can link quasiequilibrium and core-halo states (or between collisionless and collisional stages) appearing in long-range attractive interacting systems.

APPENDIX: EFFECT OF THE SIZE OF THE SYSTEM

In our cold collapse simulation, $N = 125$. However, time-evolutions of N-body systems depend on N, i.e., the size of the system [34]. Therefore, we examine the effect of the size of the system in this appendix. As a typical example, we observe a cold collapse process for $\varepsilon = -1.0$, using the system of $N = 250$ particles. The initial conditions are set to be the same as the conditions for $N = 125$, to simulate the cold collapse process. The results for $N = 250$ are averaged over 10 simulations and, therefore, its statistical fluctuations should be slightly larger than the fluctuations for $N = 125$ with 30 simulations.

Time evolutions of the number N_c of core particles and temperature T are shown in Fig. 11(a). We found that the time evolutions for $N = 250$ are similar to the evolutions for $N = 125$. However, initially ($t \lessapprox 0.03$), T for $N = 250$ increases earlier than T for $N = 125$. This is because, in our units, the crossing time $\tau_c \approx 0.1$ for $N = 250$ is shorter than $\tau_c \approx 0.2$ for $N = 125$. In principle, N_c for $N = 250$ should be larger than N_c for $N = 125$, due to the large number N of particles. However, for $t \approx 1$–3, the difference of N_c between $N = 250$ and $N = 125$ is small, since the system of 125 particles starts to form the core earlier than the system of 250 particles. After the rapid increase of N_c, N_c increases approximately logarithmically with time. In particular, the start times of logarithmic increase of N_c for $N = 125$ and $N = 250$ are approximately 7 and 8, respectively. Therefore, as expected, the start time for $N = 250$ is slightly later than the start time for $N = 125$, since the relaxation time $\tau_r \approx 0.6$ for $N = 250$ is longer than $\tau_r \approx 0.5$ for $N = 125$. Similarly, the virial ratio α for $N = 250$ gradually approaches a specific value more slowly, as shown in Fig. 11(b).

Finally, we observe time evolutions of the normalized ratio of velocity moments $V_{\rm M}$ and the Tsallis entropic parameter q. As shown in Fig. 11(c), $V_{\rm M}$ and q for $N = 250$ are consistent with those for $N = 125$, as for the other properties discussed above. Except for the initial stage ($t \lessapprox 0.1$), the time evolutions for $N = 250$ are likely later than the evolutions for $N = 125$, although the delay is not so clear. The delays observed in the system of 250 particles are expected to be related to the effect of the size of the system.

[1] J. Binney and S. Tremaine, *Galactic Dynamics* (Princeton University Press, Princeton, 1987).

[2] D. C. Heggie and P. Hut, *The Gravitational Million-Body Problem* (Cambridge University Press, Cambridge, 2003).

[3] S. J. Aarseth, *Gravitational N-Body Simulations: Tools and Algorithms* (Cambridge University Press, Cambridge, 2003).

[4] C. Tsallis, *Introduction to Nonextensive Statistical Mechanics: Approaching a Complex World* (Springer, 2009).

[5] V. A. Antonov, in *Dynamics of Star Clusters*, Proceedings of the Symposium, Princeton, NJ, May 29-June 1, 1984, edited by J. Goodman and P. Hut, Symposium sponsored by IAU. Dordrecht, D. Reidel Publishing Co. (IAU Symposium, No. 113, 1985), p. 525.

[6] D. Lynden-Bell and R. Wood, Mon. Not. R. Astron. Soc. **138**, 495 (1968).

[7] D. Lynden-Bell, Physica A **263**, 293 (1999).

[8] M. D'Agostino *et al.*, Phys. Lett. B **473**, 219 (2000).

[9] M. Schmidt, R. Kusche, T. Hippler, J. Donges, W. Kronmuller, B. von Issendorff, and H. Haberland, Phys. Rev. Lett. **86**, 1191 (2001).

[10] D. Lynden-Bell, Mon. Not. R. Astron. Soc. **136**, 101 (1967).

[11] J. L. Lebowitz and E. H. Lieb, Phys. Rev. Lett. **22**, 631 (1969).

[12] W. Thirring, Z. Phys. **235**, 339 (1970).

[13] M. K. H. Kiessling, J. Stat. Phys. **55**, 203 (1989).

[14] T. Padmanabhan, Phys. Rep. **188**, 285 (1990).

[15] H. A. Posch and W. Thirring, Phys. Rev. Lett. **95**, 251101 (2005).

[16] A. Renyi, *Probability Theory* (North-Holland, Amsterdam, 1970).

[17] C. Tsallis, J. Stat. Phys. **52**, 479 (1988).

[18] A. Plastino and A. R. Plastino, Phys. Lett. A **174**, 384 (1993).

[19] S. Abe, Phys. Lett. A **263**, 424 (1999).

[20] R. Silva Jr., A. R. Plastino, and J. A. S. Lima, Phys. Lett. A **249**, 401 (1998).

[21] R. S. Mendes and C. Tsallis, Phys. Lett. A **285**, 273 (2001).

[22] J. A. S. Lima and R. Silva, Phys. Lett. A **338**, 272 (2005).

[23] V. Latora, A. Rapisarda, and C. Tsallis, Phys. Rev. E **64**, 056134 (2001).

[24] P. H. Chavanis, Astron. Astrophys. **386**, 732 (2002).

[25] A. Taruya and M. Sakagami, Phys. Rev. Lett. **90**, 181101 (2003).

[26] A. Taruya and M. Sakagami, Mon. Not. R. Astron. Soc. **364**, 990 (2005).

[27] A. Nakamichi and M. Morikawa, Physica A **341**, 215 (2004).

[28] B. Liu and J. Goree, Phys. Rev. Lett. **100**, 055003 (2008).

[29] N. Komatsu, S. Kimura, and T. Kiwata, Phys. Rev. E **80**, 041107 (2009); J. Phys.: Conf. Ser. **201**, 012009 (2010).

[30] N. Komatsu, T. Kiwata, and S. Kimura, Phys. Rev. E **82**, 021118 (2010).
[31] I. King, Astron. J. **67**, 471 (1962); **70**, 376 (1965).
[32] O. Iguchi, Y. Sota, T. Tatekawa, A. Nakamichi, and M. Morikawa, Phys. Rev. E **71**, 016102 (2005).
[33] J. C. Carvalho *et al*., Physica A **384**, 507 (2007).
[34] I. Ispolatov and M. Karttunen, Phys. Rev. E **68**, 036117 (2003).
[35] T. E. C. Merrall and R. N. Henriksen, Astrophys. J. **595**, 43 (2003).
[36] J. Katz and I. Okamoto, Mon. Not. R. Astron. Soc. **317**, 163 (2000).
[37] P. H. Chavanis, C. Rosier, and C. Sire, Phys. Rev. E **66**, 036105 (2002).
[38] P. H. Chavanis, Astron. Astrophys. **432**, 117 (2005).
[39] P. H. Chavanis and C. Sire, Phys. Rev. E **83**, 031131 (2011).
[40] B. Stahl and M. K. H. Kiessling, Planet. Space Sci. **43**, 271 (1995).
[41] P. H. Chavanis and J. Sommeria, Mon. Not. R. Astron. Soc. **296**, 569 (1998).
[42] E. Follana and V. Laliena, Phys. Rev. E **61**, 6270 (2000).
[43] V. P. Youngkins and B. N. Miller, Phys. Rev. E **62**, 4583 (2000).
[44] P. Klinko and B. N. Miller, Phys. Lett. A **333**, 187 (2004).
[45] Y. Levin, R. Pakter, and T. N. Teles, Phys. Rev. Lett. **100**, 040604 (2008).
[46] I. Ispolatov and E. G. D. Cohen, Phys. Rev. Lett. **87**, 210601 (2001).
[47] P. H. Chavanis and I. Ispolatov, Phys. Rev. E **66**, 036109 (2002).
[48] I. Ispolatov and M. Karttunen, Phys. Rev. E **70**, 026102 (2004).
[49] C. Sire and P. H. Chavanis, Phys. Rev. E **69**, 066109 (2004).
[50] P. H. Chavanis and L. Delfini, Phys. Rev. E **81**, 051103 (2010).
[51] N. Komatsu, T. Kiwata, and S. Kimura, Book of Abstracts of the 2nd International Symposium on Multi-scale Simulations of Biological and Soft Materials (MSBSM 2011), p. 22, Kyoto, Japan (2011); N. Komatsu, Book of Abstracts: International Union of Theoretical and Applied Mechanics (IUTAM) Symposium on 50 Years of Chaos: Applied and Theoretical, pp. 76–77, Kyoto, Japan (2011), to be published in Procedia IUTAM.
[52] V. Latora, A. Rapisarda, and S. Ruffo, Phys. Rev. Lett. **83**, 2104 (1999).
[53] A. Pluchino, V. Latora, and A. Rapisarda, Continuum Mech. Thermodyn. **16**, 245 (2004).
[54] A. Campa, P. H. Chavanis, A. Giansanti, and G. Morelli, Phys. Rev. E **78**, 040102(R) (2008).
[55] F. Baldovin, P. H. Chavanis, and E. Orlandini, Phys. Rev. E **79**, 011102 (2009).
[56] F. Staniscia, P. H. Chavanis, G. De Ninno, and D. Fanelli, Phys. Rev. E **80**, 021138 (2009).
[57] D. Fanelli, M. Merafina, and S. Ruffo, Phys. Rev. E **63**, 066614 (2001).
[58] N. Komatsu, T. Kiwata, and S. Kimura, Physica A **387**, 2267 (2008); **388**, 1344 (2009); **388**, 639 (2009).
[59] We selected this fitting procedure, since the obtained result was better than the result obtained from other simple procedures.
[60] For the initial setup, we prepare the system for $\varepsilon = -0.6$ with a Gaussian-like velocity distribution as follows: (1) We first prepare self-gravitating systems at an approximate virial equilibrium state for $\varepsilon = -0.2$. Since $\varepsilon = -0.2$ is sufficiently above the collapse energy $\varepsilon_{\rm coll} \approx -0.339$, the velocity distribution at the approximate virial equilibrium state is expected to be a Gaussian-like distribution. To obtain the approximate virial equilibrium state and the Gaussian-like velocity distribution, the microcanonical ensemble simulation is continued over 10 units of time [29,30]. We have confirmed that the obtained system is in the approximate virial equilibrium state and that the obtained velocity distribution is a Gaussian-like distribution. (2) For the initial setup, the initial density profile is set to be the above obtained density profile. The obtained Gaussian-like velocity distribution is rescaled in order to set the total energy as $\varepsilon = -0.6$. That is, the initial velocity distribution is set to be the rescaled velocity distribution. We have confirmed that the initial velocity distribution is a Gaussian-like distribution. (The initial potential and kinetic energies are $\varepsilon_{\rm PE0} = -0.800 \pm 0.052$, $\varepsilon_{\rm KE0} = 0.200 \pm 0.052$, respectively.) Ensemble simulations for $\varepsilon = -0.6$ are carried out, using the above initial setup. Note that this simulation is slightly different from the cold collapse simulation, since the initial temperature corresponding to the kinetic energy is not so low.
[61] The initial temperature for $\varepsilon = -0.2$ is $T_0 = 0.422 \pm 0.009$ and, therefore, the initial velocity speed $\mathbf{v}_0$ is not negligible unlike for the cold collapse simulation. That is, the initial velocity distribution is a water-bag-like distribution rather than a delta-function-like distribution, since all the particles are set to have a velocity with equal $\mathbf{v}_0$ but with a random direction.
[62] If we assume a q'-Gaussian speed distribution, we can obtain a similar exact relation $V_{\rm Mex}(q')$. However, similarly, we cannot directly compare between the exact relation $V_{\rm Mex}(q')$ and the simulated relation of $V_{\rm M}$ to q. This is because q values discussed in this study are not equal to the above q' values, since q is obtained from fitting with the simulated velocity distribution.
[63] M. Trenti and G. Bertin, Astron. Astrophys. **429**, 161 (2005).
[64] C. Nipoti, P. Londrillo, and L. Ciotti, Astrophys. J. **660**, 256 (2007).